

Quantum dots on the InAs(110) cleavage surface created by atom manipulation

Van Dong Pham ^{1,*}, Yi Pan ^{1,2,*}, Steven C. Erwin ³, and Stefan Fölsch ^{1,†}

¹*Paul-Drude-Institut für Festkörperelektronik, Hausvogteiplatz 5-7, Leibniz-Institut im Forschungsverbund Berlin e. V., 10117 Berlin, Germany*

²*Center for Spintronics and Quantum Systems, State Key Laboratory for Mechanical Behavior of Materials, Xi'an Jiaotong University, Xi'an 710049, China*

³*Center for Computational Materials Science, Naval Research Laboratory, Washington, DC 20375, USA*



(Received 21 November 2023; accepted 14 February 2024; published 12 March 2024)

Cryogenic scanning tunneling microscopy was employed in combination with density-functional theory calculations to explore quantum dots made of In adatoms on the InAs(110) surface. Each adatom adsorbs at a surface site coordinated by one cation and two anions, and transfers one electron to the substrate, creating an attractive quantum well for electrons at the surface. We used the scanning-probe tip to assemble the positively charged adatoms into precisely defined quantum dots exhibiting a bound state roughly 0.1 eV below the Fermi level at an intrinsic linewidth of only ~ 4 meV, as revealed by scanning tunneling spectroscopy. For quantum-dot dimers, we observed the emergence of a bonding and an antibonding state with even and odd wave-function character, respectively, demonstrating the capability to engineer quasimolecular electronic states. InAs(110) constitutes a promising platform in this respect because highly perfect surfaces can be readily prepared by cleavage and charged adatoms can be generated *in situ* by the scanning-probe tip.

DOI: [10.1103/PhysRevResearch.6.013269](https://doi.org/10.1103/PhysRevResearch.6.013269)

I. INTRODUCTION

Semiconductor quantum dots play a central role in optoelectronic device applications [1]. At the level of fundamental research, they make it possible to explore superimposed and entangled quantum states [2,3], semiconductor qubits [4], electron correlation in artificial lattices [5], and electronic quantum transport [6], to mention only a few. Aside from their fabrication in the form of colloidal crystals [7], quantum dots are typically created in semiconductor heterostructures by growing vertically and laterally aligned nanocrystals [2,3,8,9], by imposing lateral confinement using electron-beam lithography [5,10], or by depleting a two-dimensional electron gas (2DEG) using external gates [11,12] and local oxidation [13].

The method of 2DEG depletion using external gates exploits the electric field effect to spatially modulate the carrier density. In our previous work [14], we followed a similar idea of spatially controlling the electrostatic surface potential; however, at the level of single atoms: we used the tip of a scanning tunneling microscope to assemble short atomic chains on an InAs(111)A surface by atom manipulation [15]. The chains consisted of six positively charged In adatoms leading to electronic confinement, and hence, the emergence of a bound state with discrete energy—the fingerprint of a quantum dot. We showed that these dots can be arranged

and thereby coupled in various ways, yielding quasimolecular electronic states, which can be described by a tight-binding Hamiltonian assuming a single *s* orbital on each site [14,16].

Here, we extend this concept to the (110) cleavage surface of indium arsenide. First, the adsorption and charge state of an In adatom on InAs(110) are investigated by scanning tunneling microscopy (STM) and complementary density-functional theory (DFT) calculations. It is then demonstrated that an assembly of six adatoms confines electrons and thus behaves like a quantum dot. The resulting bound state has an intrinsic linewidth of ~ 4 meV, which is remarkably small for confined electronic states at surfaces. Finally, it is shown that quantum-dot dimers can be created, leading to bonding and antibonding states as verified by scanning tunneling spectroscopy (STS). The present findings are important because they facilitate the STM-based construction of quantum structures on a new InAs platform: a cleaved (110) surface is significantly easier to prepare than a (111)A-terminated surface requiring a dedicated growth facility for molecular beam epitaxy (MBE) [17]. Moreover, working in (110) surface orientation offers the prospect of exploring cleaved III-V semiconductor heterostructures in cross-sectional geometry to ultimately be able to create electrical gating of the STM-generated nanostructures.

II. RESULTS AND DISCUSSION

The STM investigations were carried out in ultrahigh vacuum (UHV) at a sample temperature of 5 K. We used undoped and (001)-oriented InAs wafers cleaved in UHV to obtain the InAs(110) surface. The left panel in Fig. 1(a) shows a constant-current topography image of an In adatom adsorbed on the InAs(110) surface. At the sample bias of 0.1 V as applied here, the surface As atoms are imaged as protrusions

*These authors contributed equally to this work.

†foelsch@pdi-berlin.de

Published by the American Physical Society under the terms of the [Creative Commons Attribution 4.0 International](https://creativecommons.org/licenses/by/4.0/) license. Further distribution of this work must maintain attribution to the author(s) and the published article's title, journal citation, and DOI.

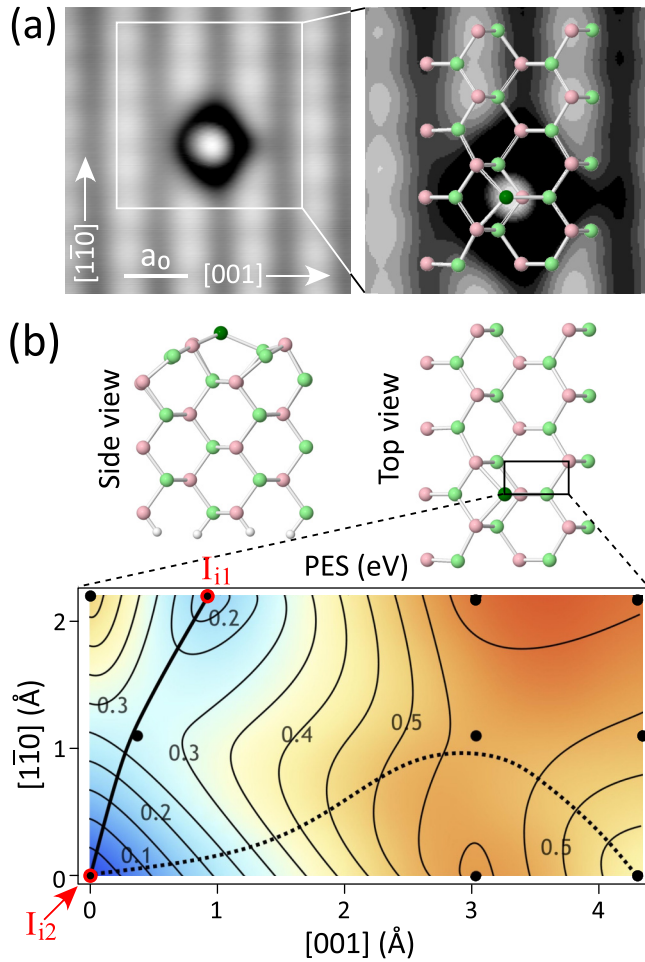


FIG. 1. (a) Left: STM image (1 nA, -0.6 V) of an In adatom on InAs(110) located within the channel between rows of surface As atoms imaged as protrusions; row spacing: $a_0 = 6.06$ Å. Right: close-up view at staggered gray scale with overlaid structure model showing the surface In (green) and As atoms (pink) as well as the In adatom (dark green). (b) Top: structural model in top and side views as determined by DFT. Bottom: DFT potential-energy surface (PES) for an In adatom diffusing on InAs(110); the solid line shows the minimum energy path between the stable (I_2) and metastable (I_1) configurations along the channel whereas the dotted line indicates the barrier across the channel. At each black point within the rectangle, the x and y positions of the adatom were held fixed while all other atomic coordinates (including the first four InAs layers) were relaxed.

arranged in rows along the $[1\bar{1}0]$ in-plane direction [18]; the spacing between the rows is $a_0 = 6.06$ Å, the cubic lattice constant of InAs. The adatom in the center of the image is located in the channel in between the rows, consistent with previous work [19,20] predicting interstitial configurations in which the adatom is bonded either to two cations and one anion (labeled I_{11}) or to two anions and one cation (I_{12}). In agreement with the findings by Weber *et al.* [20], our DFT calculations confirm that I_{12} is the most stable configuration, as illustrated by the right-hand side panel showing a close-up view together with an overlaid structure model. [The orientation of the structure model with respect to the (001) plane is

confirmed experimentally by the chemical contrast between surface anions and cations (Supplemental Material [21], Fig. S1)—first revealed by the atom-selective STM imaging of GaAs(110) [22]].

We performed DFT calculations to determine the equilibrium geometry of InAs(110) with and without adsorbed In adatoms, as well as the potential-energy surface for surface diffusion of those adatoms (general details on the calculations are given in Ref. [14]). Figure 1(b) shows the DFT potential-energy surface for an In adatom diffusing on the InAs(110) cleavage surface and provides quantitative information on the adsorption behavior: the metastable configuration I_{11} is 0.2 eV higher in energy than the stable configuration I_{12} . The diffusion barrier along the channel is 0.3 eV (the minimum energy path is sketched as a solid curve); this barrier can be overcome above ~ 120 K. On the other hand, the barrier across the channel is about 0.6 eV (dotted curve) and can be overcome above ~ 240 K. However, this pathway is probably preempted by exchange between the adatom and a surface In atom, similar to the exchange reaction previously observed for Mn substitutional impurities on InAs(110) [23].

We probed the electronic surface properties by STS measurements of the tunnel conductance dI/dV , which provides an approximate measure of the electronic density of states. The spectrum shown in blue in Fig. 2(a) was recorded with the tip probing the bare surface. It reveals the energy band gap of InAs (0.42 eV at the measurement temperature of 5 K [24]) and, most prominently, Fermi-level pinning in the conduction band. (The residual conductance observed within the band gap is due to the so-called “dopant-induced” contribution arising from electrons tunneling out of the filled conduction-band states located near the band edge [25]). Fermi-level pinning in the conduction band is a generic feature of InAs surfaces, indicating charge accumulation at the surface [20]. In agreement with previous STS work on cleaved InAs(110) [18], we observe conductance peaks near the conduction-band minimum just below the Fermi level (at sample bias $V=0$), which are a manifestation of conduction-band states that undergo vertical confinement—and thereby quantization—because of the downward band bending near the surface. In the blue spectrum in Fig. 2(a), these states show up as two peaks at -30 and -11 mV, respectively, reflecting the two lowest subbands of the accumulation layer (denoted s_1 and s_2). The actual energy and magnitude of the peaks observed depends on the location probed by the tip (see Fig. S2 in the Supplemental Material [21]). We attribute this spatial variation to the effect of electrostatic disorder due to defects [26–28] in the surface-near region.

The red spectrum in Fig. 2(a) was recorded with the tip probing a single In adatom on InAs(110) and reveals a conductance peak at a sample bias of 0.85 V. The corresponding state derives predominantly from $5p$ atomic orbital states of the adatom as evident from the density of states calculated by DFT [see Fig. 2(b)]. It is noted that a similar adatom-induced state was observed previously for In adatoms on InAs(111)A [29] and GaSb(110) [30].

Similar to the situation observed on InAs(111)A, In adatoms on InAs(110) are positively charged. This is evident from the increased apparent height around the charged adatom when imaged at positive sample bias as in the upper panel of

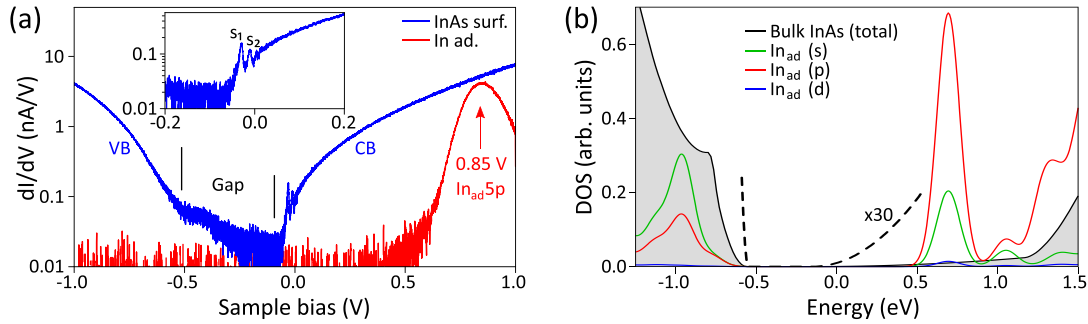


FIG. 2. (a) Conductance spectra on a logarithmic scale recorded with the tip probing the bare surface (blue, set-point parameters prior to opening the feedback loop: 5 nA, 1 V) and a discrete In adatom (red, set point: 1 nA, 1 V). The blue spectrum indicates Fermi-level pinning in the conduction band (CB) and the presence of accumulation-layer states denoted s_1 and s_2 near the CB minimum (see inset); the red spectrum reveals an adatom-derived unoccupied state at 0.85 eV. Root-mean-square (rms) value of the lock-in modulation for all spectra: $V_{\text{mod}} = 1.8$ mV. (b) Electronic structure of In on InAs(110) calculated by DFT with the Heyd-Scuseria-Ernzerhof screened hybrid functional; projected bulk bands are gray (scaled up to highlight the band onsets; see dashed line); the zero of energy was set 100 meV above the CB minimum. Colored curves show the total density of states projected onto the s -, p -, and d -valence orbitals of the adatom; the experimental state at 0.85 eV derives predominantly from $5p$ atomic orbital states.

Fig. 3(a). The increased height is due to the screened Coulomb potential induced by the charged adatom, which locally increases the density of states available for the tunnel process [31,32]. It is noteworthy that the hillock produced by the local potential is not symmetric about the adatom position. This asymmetry is clearly evident from the topographic line scan in the lower panel of Fig. 3(a) taken along the dashed line.

To explain this observation, we consider the DFT electrostatic potential in a plane just above the surface. A contour plot of the potential, 3 Å above the surface and within the rectangular area marked in the STM image, is shown in the upper panel of Fig. 3(b). Far from the adatom, the local potential reflects the fact that electrons are transferred from surface In atoms to surface As atoms in accordance with the electron counting rule [33]. The defect complex consisting of the In adatom plus the surface In atom to its left transfers one electron to the environment, creating a localized positive charge that is attractive for electrons. The line scan in the lower panel of Fig. 3(b) shows the contributions from the adatom and the surface In atom. The double-atom structure of this defect complex explains the asymmetry observed in STM topography. Moreover, the DFT electrostatic potential in the lower panel of Fig. 3(b) is consistent with the experimentally determined local potential, which can be extracted from the bias offset in I - V curves measured close to the charged point defect [34,35] (Supplemental Material [21], Fig. S3).

In contrast to the MBE-grown InAs(111)A surface [36], cleaved InAs(110) is free of native adatoms. Nevertheless, individual In atoms can be transferred from the scanning-probe tip to the surface [37] after proper preconditioning (In agglomeration at the tip apex [38]) and subsequently repositioned by lateral atom manipulation (Supplemental Material [21], Fig. S4). This method was used in Fig. 4(a) to arrange $N=6$ adatoms into a hexagon having a width of $7a_0 = 42.42$ Å along [001] and $8a_0/\sqrt{2} = 34.28$ Å along the $[1\bar{1}0]$ direction. The upper panel of Fig. 4(b) shows a set of size-dependent conductance spectra intermediately recorded at the tip position marked in the STM image in Fig. 4(a) while building up the hexagon one adatom after another. Starting from the bare surface [$N=0$; same spectrum as in Fig. 2(a)], it is seen that a

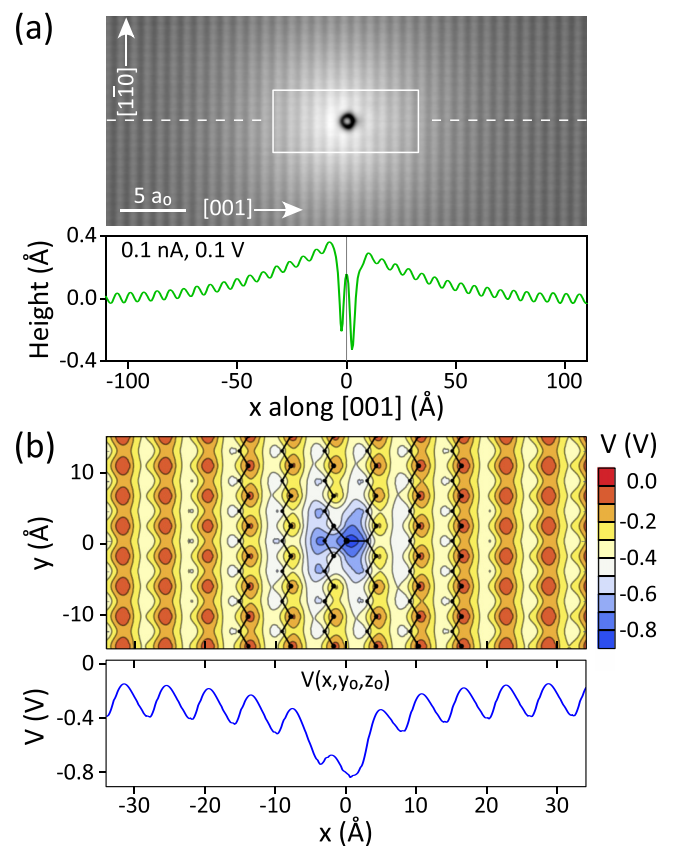


FIG. 3. (a) Upper panel: larger-scale STM image (0.1 nA, 0.1 V) of an In adatom on InAs(110); the increased apparent height around the positively charged adatom arises from its screened Coulomb potential. Lower panel: measured height contour taken along the dashed line in (a) showing that the local band bending is asymmetric about the adatom position. (b) Upper panel: DFT electrostatic potential 3 Å above the surface inside the rectangular box in (a). Blue shading is more strongly attractive for electrons. The In adatom and the adjacent In surface atom together have a net positive charge $+1e$, explaining the experimentally observed asymmetry. Lower panel: line scan of the calculated potential $V(x, y_0, z_0)$ showing the two separate contributions from the adatom and the surface In atom.

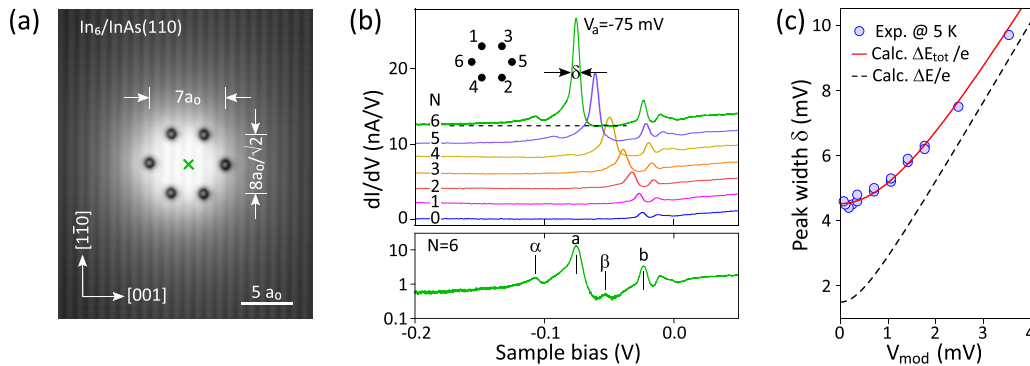


FIG. 4. (a) STM image (0.1 nA, 0.1 V) of six In adatoms on InAs(110) assembled into a hexagon (“dot”) $7a_0 = 42.42 \text{ \AA}$ wide and $8a_0/\sqrt{2} = 34.28 \text{ \AA}$ tall; the increased apparent height is due to the Coulomb potential arising from the adatoms. (b) Upper panel: size-dependent conductance spectra (set point: 1 nA, 0.3 V; $V_{\text{mod}} = 1.8 \text{ mV}$) with N the number of adatoms in the dot (assembly sequence highlighted by the inset): a strong peak evolves at $V_a = -75 \text{ mV}$ for the complete hexagon ($N=6$) together with smaller peaks at higher and lower energies; the width δ of the main peak (full width at half maximum) is measured relative to the dashed horizontal baseline. Lower panel: logarithmic plot of the $N=6$ spectrum; peaks denoted α and β are replicas of peaks a and b induced by inelastic electron tunneling. (c) Measured peak width δ (blue symbols) versus lock-in modulation voltage V_{mod} (root-mean-square value); the dashed curve indicates the resolution limit $\Delta E/e$ while the red curve is the calculated peak width $\Delta E_{\text{tot}}/e$ assuming an intrinsic linewidth $\Gamma = 4.3 \text{ meV}$ of the corresponding state.

strong conductance peak evolves for the completed hexagon ($N=6$), revealing a bound state 75 meV below the Fermi level. Moreover, a number of smaller peaks and a line-shape asymmetry of the strong peak are observed as readily seen in the logarithmic plot of the $N=6$ spectrum in the lower panel of Fig. 4(b); these features will be addressed in more detail below. Note also that all spectral features observed here were reproduced for various independently assembled dots in different experimental runs.

These spectra demonstrate that the attractive potential induced by the assembled adatoms confines electrons at the cleaved InAs(110) surface. Hence, the hexagon acts as a quantum dot—an “artificial atom”—that creates a bound state of discrete energy. [It is noted that electron confinement was reported recently also for Cs adatom structures created by atom manipulation on the InSb(110) surface [39]]. We have not yet identified the detailed physical origin of the bound state showing up as the dominant peak in the topmost spectrum for $N=6$, that is to say, it remains to be shown whether it originates from surface-accumulated (bulk) conduction-band states or if also other surface states are involved. Further investigations are required to establish precisely which states are confined in the present case; the central finding of this work is that quantum dots can be assembled from charged In adatoms on the cleaved InAs(110) surface.

Returning to the logarithmic plot in Fig. 4(b), the conductance peaks labeled α and β are correlated to those labeled a and b : the difference in bias voltage at which they occur is $V_a - V_\alpha = 32 \text{ mV}$ and, similarly, $V_b - V_\beta = 30 \text{ mV}$. This suggests that α and β are replicas of a and b , respectively, induced by inelastic electron tunneling. The corresponding energy transfer observed here is consistent with the excitation of optical phonons implying a transfer of 29 meV as found previously by Chen *et al.* [40] who carried out high-resolution electron-energy loss spectroscopy (HREELS) measurements on cleaved InAs(110). The same authors observed a broaden-

ing of the quasielastic HREELS peak, which they attributed to plasmonic excitations. We propose that the same inelastic process leads to the asymmetric line shape observed in our experiment, which is most obvious from the bound-state peak labeled a in Fig. 4(b). These effects are experimentally accessible in the present system because of the narrow line width of the bound state, which will be explored next.

We deduced the linewidth from tunnel conductance measurements at varying energy resolution by recording peak profiles at different root-mean-square values V_{mod} of the lock-in modulation voltage and found that the profile steadily sharpens as V_{mod} is reduced. At successively small modulations, the measured peak width δ (the full width at half maximum [41]) converged to a value well below 5 mV as evident from the data points collected in Fig. 4(c). The theoretical energy resolution [42] is $\Delta E = \sqrt{(3.5kT)^2 + (2.5eV_{\text{mod}})^2}$, where the two terms in the square root take into account the broadening due to temperature and lock-in modulation, respectively. The black dashed line in Fig. 4(c) shows the quantity $\Delta E/e$ at the measurement temperature of 5 K . On the other hand, a state with intrinsic linewidth Γ is expected to be observed at a total energy broadening of $\Delta E_{\text{tot}} = \sqrt{(3.5kT)^2 + (2.5eV_{\text{mod}})^2 + \Gamma^2}$ [43]. The quantity $\Delta E_{\text{tot}}/e$ defined by the latter expression yields a good fit of the data points at an intrinsic linewidth of $\Gamma = 4.3 \text{ meV}$ as shown by the full red curve in Fig. 4(c).

Quite generally, the linewidth Γ is inversely proportional to the lifetime of carriers, which is limited by inelastic (electron-electron and electron-phonon) scattering and—in the case of confined states—lossy scattering due to partial reflectance at the confining boundary [44]. Given the small spatial extent of the confining potential considered here (on the order of 50 \AA), it appears likely that lossy scattering plays a significant role in our In₆ dots. In turn, this would imply that even longer lifetimes could be obtained for deeper and/or wider potential wells created from In adatoms on InAs(110).

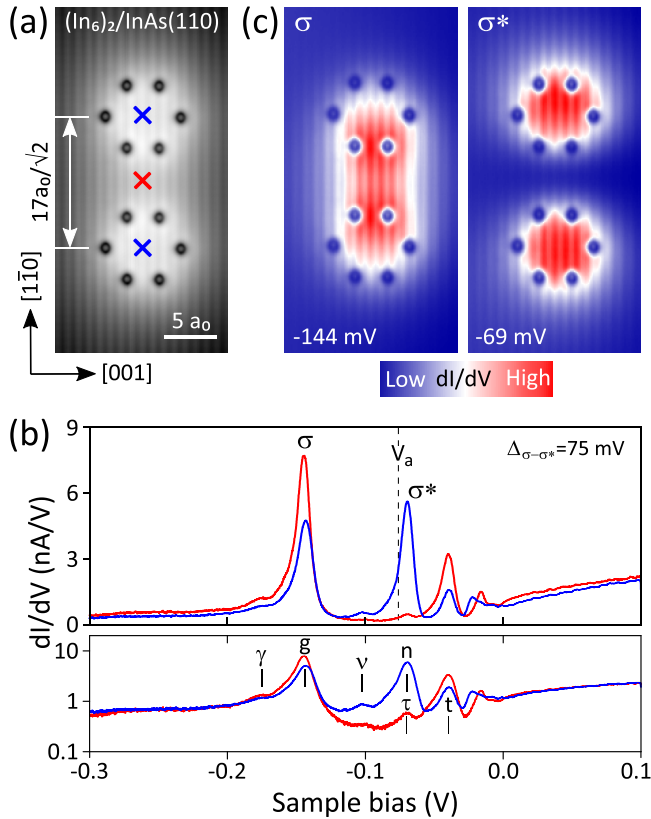


FIG. 5. (a) STM image (0.1 nA, 0.1 V) of the same dot as in Fig. 4 (a) after adding another dot of identical structure at a center-to-center spacing of $17a_0/\sqrt{2} = 72.85 \text{ \AA}$ along $[1\bar{1}0]$. (b) Upper panel: spectra recorded with the tip placed above (blue, average of equivalent spectra taken on either dot) and in between the dots (red); two major peaks labeled σ and σ^* are observed together with smaller peaks (set point: 0.2 nA, 0.1 V); the vertical dashed line marks the peak position initially observed for the single dot. Lower panel: logarithmic plot of the same spectra featuring replicas of conductance peaks due to inelastic electron tunneling. All spectra taken at set-point parameters 0.2 nA, 0.1 V, and $V_{\text{mod}} = 1.8 \text{ mV}$. (c) Spatial conductance maps ($V_{\text{mod}} = 3.5 \text{ mV}$) recorded at constant tip height and the sample biases where the σ and σ^* peaks are observed in (b), confirming the bonding (left) and antibonding character (right) of the corresponding states of the dimer.

Finally, we demonstrate that quasimolecular electronic states can be created by bound-state coupling in quantum-dot dimers created on the InAs(110) cleavage surface. In the topography image displayed in Fig. 5(a), we started from the same dot as in Fig. 4(a) and added an identical dot at a center-to-center spacing of $17a_0/\sqrt{2} = 72.85 \text{ \AA}$ along the $[1\bar{1}0]$ direction, yielding a quantum-dot dimer. The corresponding spectra in Fig. 5(b) were recorded with the tip placed above (blue) and in between the dots (red). They reveal the emergence of a bonding (σ) and an antibonding state (σ^*) as expected for the symmetric and antisymmetric superposition of the bound states belonging to the two dots. The observed σ - σ^* splitting measures $\Delta_{\sigma-\sigma^*} = 75 \text{ mV}$. Note also that the σ - σ^* doublet is downshifted from the energy of the single dot indicated by the dashed line; this shift arises from the

electrostatic potential change that each dot experiences from the other as previously observed in quantum-dot dimers on InAs(111)A [16]. Aside from the dominant σ and σ^* peaks in the conductance spectra, we again observe a set of smaller peaks at higher and lower energies as detailed in the lower panel of Fig. 5(b). Again, the spectra feature inelastic replicas consistent with the excitation of surface phonons [40]; this is evident from the bias-voltage differences of 31, 33, and 30 mV found for the conductance-peak pairs (γ, g), (ν, n), and (τ, t), respectively. To further analyze the bonding and antibonding states, Fig. 5(c) displays spatial conductance maps recorded at the corresponding bias voltages of the σ and σ^* peaks in panel (b), respectively. These maps are consistent with the symmetric (σ) and antisymmetric (σ^*) wave-function character of the bonding and antibonding states.

III. CONCLUSIONS

We employed cryogenic STM and STS measurements in combination with DFT calculations to perform an in-depth study of individual In adatoms on the InAs(110) cleavage surface. The adatom is found to adsorb in the channel between the rows of surface atoms along the $[1\bar{1}0]$ in-plane direction and is bonded to two anions and one cation (I_{i2} configuration), in agreement with previous theoretical work [20]. The I_{i1} configuration (bonding to two cations and one anion) is metastable and 0.2 eV higher in energy. It is found that the adatom and its neighboring surface In atom along the $[00\bar{1}]$ in-plane direction are positively charged, with a net charge of $+1e$. By arranging these charged adatoms into groups with atomic precision, we have created quantum dots that laterally confine electrons at the surface. For the bound state resulting from this confinement, we found an intrinsic linewidth of only $\sim 4 \text{ meV}$. (The linewidths observed in conductance spectra of confined electrons on metal surfaces are typically larger by a factor of 10 to 10^2 [45,46].) Finally, it was demonstrated that the quantum coupling between two identical dots placed side by side leads to the emergence of a bonding and an antibonding state indicating the symmetric and antisymmetric superposition of the dot wave functions.

The comparably small intrinsic linewidth observed for the bound state of atomic-scale quantum dots on InAs(110) will open the way to resolve the energy-level spectrum of more elaborate quantum-dot arrays hosting exotic electronic states [47,48]. The system presented here has the practical advantage that large-scale and atomically flat surface terraces are readily prepared by cleavage in UHV and no extra deposition of material is required to generate charged adatoms, making it a promising platform for the creation of semiconductor quantum structures by scanning-probe techniques.

ACKNOWLEDGMENTS

V.D.P., Y.P., and S.F. acknowledge funding by the Deutsche Forschungsgemeinschaft (DFG, German Research Foundation) under Grants No. FO362/4-2 and No. 437494632. Y.P. also acknowledges the National Natural Science Foundation of China (Grant No. 12074302) for supporting the

collaboration. S.C.E. was supported by the Office of Naval Research through the Naval Research Laboratory's Basic

Research Program. We gratefully acknowledge fruitful discussions with Klaus Biermann and Randall M. Feenstra.

- [1] P. Yu and Z. M. Wang, *Quantum Dot Optoelectronic Devices* (Springer, Cham, 2020).
- [2] G. Schedelbeck, W. Wegscheider, M. Bichler, and G. Abstreiter, Coupled quantum dots fabricated by cleaved edge overgrowth: From artificial atoms to molecules, *Science* **278**, 1792 (1997).
- [3] M. Bayer, P. Hawrylak, K. Hinzer, S. Fafard, M. Korkusinski, Z. R. Wasilewski, O. Stern, and A. Forchel, Coupling and entangling of quantum states in quantum dot molecules, *Science* **291**, 451 (2001).
- [4] A. Chatterjee, P. Stevenson, S. De Franceschi, A. Morello, N. P. de Leon, and F. Kuemmeth, Semiconductor qubits in practice, *Nat. Rev. Phys.* **3**, 157 (2021).
- [5] A. Singha, M. Gibertini, B. Karmakar, S. Yuan, M. Polini, G. Vignale, M. I. Katsnelson, A. Pinczuk, L. N. Pfeiffer, K. W. West, and V. Pellegrini, Two-dimensional Mott-Hubbard electrons in an artificial honeycomb lattice, *Science* **332**, 1176 (2011).
- [6] L. P. Kouwenhoven, D. G. Austing, and S. Tarucha, Few-electron quantum dots, *Rep. Prog. Phys.* **64**, 701 (2001).
- [7] R. Rossetti, S. Nakahara, and L. E. Brus, Quantum size effects in the redox potentials, resonance Raman spectra, and electronic spectra of CdS crystallites in aqueous solution, *J. Chem. Phys.* **79**, 1086 (1983).
- [8] Z. R. Wasilewski, S. Fafard, and J. P. McCaffrey, Size and shape engineering of vertically stacked self-assembled quantum dots, *J. Cryst. Growth* **201-202**, 1131 (1999).
- [9] L. Wang, A. Rastelli, S. Kiravittaya, M. Benyoucef, and O. G. Schmidt, Quantum dots: Self-assembled quantum dot molecules, *Adv. Mater.* **21**, 2601 (2009).
- [10] M. A. Reed, J. N. Randall, R. J. Aggarwal, R. J. Matyi, T. M. Moore, and A. E. Wetsel, Observation of discrete electronic states in a zero-dimensional semiconductor nanostructure, *Phys. Rev. Lett.* **60**, 535 (1988).
- [11] T. H. Oosterkamp, T. Fujisawa, W. G. van der Wiel, K. Ishibashi, R. V. Hijman, S. Tarucha, and L. P. Kouwenhoven, Microwave spectroscopy of a quantum-dot molecule, *Nature (London)* **395**, 873 (1998).
- [12] T. Fujisawa, T. H. Oosterkamp, W. G. van der Wiel, B. W. Broer, R. Aguado, S. Tarucha, and L. P. Kouwenhoven, Spontaneous emission spectrum in double quantum dot devices, *Science* **282**, 932 (1998).
- [13] A. Fuhrer, A. Dorn, S. Lüscher, T. Heinzl, K. Ensslin, W. Wegscheider, and M. Bichler, Electronic properties of nanostructures defined in Ga[Al]As heterostructures by local oxidation, *Superlattices Microstruct.* **31**, 19 (2002).
- [14] S. Fölsch, J. Martínez-Blanco, J. Yang, K. Kanisawa, and S. C. Erwin, Quantum dots with single-atom precision, *Nat. Nanotechnol.* **9**, 505 (2014).
- [15] J. A. Stroscio and D. M. Eigler, Atomic and molecular manipulation with the scanning tunneling microscope, *Science* **254**, 1319 (1991), and references therein.
- [16] V. D. Pham, Y. Pan, S. C. Erwin, F. von Oppen, K. Kanisawa, and S. Fölsch, Topological states in dimerized quantum-dot chains created by atom manipulation, *Phys. Rev. B* **105**, 125418 (2022).
- [17] K. D. Vallejo, T. A. Garrett, K. E. Sautter, K. Saythavy, B. Liang, and P. J. Simmonds, InAs(111)A homoepitaxy with molecular beam epitaxy, *J. Vac. Sci. Technol. B* **37**, 061810 (2019), and references therein.
- [18] J. Klijn, L. Sacharow, C. Meyer, S. Blügel, M. Morgenstern, and R. Wiesendanger, STM measurements on the InAs(110) surface directly compared with surface electronic structure calculations, *Phys. Rev. B* **68**, 205327 (2003).
- [19] A. Höglund, C. W. M. Castleton, M. Göthelid, B. Johansson, and S. Mirbt, Point defects on the (110) surfaces of InP, InAs, and InSb: A comparison with bulk, *Phys. Rev. B* **74**, 075332 (2006).
- [20] J. R. Weber, A. Janotti, and C. G. Van de Walle, Intrinsic and extrinsic causes of electron accumulation layers on InAs surfaces, *Appl. Phys. Lett.* **97**, 192106 (2010), and references therein.
- [21] See Supplemental Material at <http://link.aps.org/supplemental/10.1103/PhysRevResearch.6.013269> for additional information on chemical contrast in STM imaging, spectra of accumulation-layer states, the local electrostatic potential, and the manipulation of adatoms.
- [22] R. M. Feenstra, J. A. Stroscio, J. Tersoff, and A. P. Fein, Atom-selective imaging of the GaAs(110) surface, *Phys. Rev. Lett.* **58**, 1192 (1987).
- [23] Y. J. Song, S. C. Erwin, G. M. Rutter, P. N. First, N. B. Zhitenev, and J. A. Stroscio, Making Mn substitutional impurities in InAs using a scanning tunneling microscope, *Nano Lett.* **9**, 4333 (2009).
- [24] Z. M. Fang, K. Y. Ma, D. H. Jaw, R. M. Cohen, and G. B. Stringfellow, Photoluminescence of InSb, InAs, and InAsSb grown by organometallic vapor phase epitaxy, *J. Appl. Phys.* **67**, 7034 (1990).
- [25] R. M. Feenstra, Tunneling spectroscopy of the (110) surface of direct-gap III-V semiconductors, *Phys. Rev. B* **50**, 4561 (1994).
- [26] A. L. Efros, Metal-non-metal transition in heterostructures with thick spacer layers, *Solid State Commun.* **70**, 253 (1989).
- [27] C. Metzner, M. Hofmann, and G. H. Döhler, Intersubband transitions of a quasi-two-dimensional electron gas in the strong disorder regime, *Phys. Rev. B* **58**, 7188 (1998).
- [28] S. Perraud, K. Kanisawa, Z.-Z. Wang, and T. Fujisawa, Imaging the percolation of localized states in a multisubband two-dimensional electronic system subject to a disorder potential, *Phys. Rev. B* **76**, 195333 (2007).
- [29] S. Fölsch, J. Yang, C. Nacci, and Kiyoshi Kanisawa, Atom-by-atom quantum state control in adatom chains on a semiconductor, *Phys. Rev. Lett.* **103**, 096104 (2009).
- [30] K. Suzuki, K. Onomitsu, and K. Kanisawa, Tunneling spectroscopy of an indium adatom precisely manipulated on the cross-sectional surface of InAs/GaSb quantum structures, *Phys. Rev. B* **100**, 235306 (2019).

- [31] J. A. Stroscio, R. M. Feenstra, and A. P. Fein, Local state density and long-range screening of adsorbed oxygen atoms on the GaAs(110) surface, *Phys. Rev. Lett.* **58**, 1668 (1987).
- [32] J. F. Zheng, X. Liu, N. Newman, E. R. Weber, D. F. Ogletree, and M. Salermon, Scanning tunneling microscopy studies of Si donors (Si_{Ga}) in GaAs, *Phys. Rev. Lett.* **72**, 1490 (1994).
- [33] The electron counting rule implies a redistribution of charge among broken surface bonds such that anion surface orbitals have lone pairs, while cation surface orbitals are empty.
- [34] K. Teichmann, M. Wenderoth, S. Loth, R. G. Ulbrich, J. K. Garleff, A. P. Wijnheijmer, and P. M. Koenraad, Controlled charge switching on a single donor with a scanning tunneling microscope, *Phys. Rev. Lett.* **101**, 076103 (2008).
- [35] J. Yang, S. C. Erwin, K. Kanisawa, C. Nacci, and Stefan Fölsch, Emergent multistability in assembled nanostructures, *Nano Lett.* **11**, 2486 (2011).
- [36] A. Taguchi and K. Kanisawa, Stable reconstruction and adsorbates of InAs(111)A surface, *Appl. Surf. Sci.* **252**, 5263 (2006).
- [37] K. Suzuki, S. Fölsch, and K. Kanisawa, Assembling indium atoms into nanostructures on a cleaved InAs(110) surface, *Appl. Phys. Express* **4**, 085002 (2011).
- [38] J. Yang, C. Nacci, J. Martínez-Blanco, K. Kanisawa, and S. Fölsch, Vertical manipulation of native adatoms on the InAs(111)A surface, *J. Phys.: Condens. Matter* **24**, 354008 (2012).
- [39] E. Sierda, X. Huang, D. I. Badrtdinov, B. Kiraly, E. J. Knol, G. C. Groenenboom, M. I. Katsnelson, M. Rösner, D. Wegner, and A. A. Khajetoorians, Quantum simulator to emulate lower-dimensional molecular structure, *Science* **380**, 1048 (2023).
- [40] Y. Chen, J. C. Hermanson, and G. J. Lapeyre, Coupled plasmon and phonon in the accumulation layer of InAs(110) cleaved surfaces, *Phys. Rev. B* **39**, 12682 (1989).
- [41] For a direct measurement of the full width at half maximum δ , we defined a constant baseline adjusted to the approximately constant background signal at the right-hand side footing of the conductance-peak [see the dashed horizontal line in Fig. 4(b)].
- [42] M. Morgenstern, Probing the local density of states of dilute electron systems in different dimensions, *Surf. Rev. Lett.* **10**, 933 (2003).
- [43] Expressing the quantities ΔE and ΔE_{tot} as a sum of variances is strictly valid only for Gaussian broadening and thereby of approximate character in the general case.
- [44] J. Kröger, L. Limot, H. Jensen, R. Berndt, S. Crampin, and E. Pehlke, Surface state electron dynamics of clean and adsorbate-covered metal surfaces studied with the scanning tunnelling microscope, *Prog. Surf. Sci.* **80**, 26 (2005).
- [45] A. A. Khajetoorians, D. Wegner, A. F. Otte, and I. Swart, Creating designer quantum states of matter atom-by-atom, *Nat. Rev.* **1**, 703 (2019), and references therein.
- [46] L. Yan and P. Liljeroth, Engineered electronic states in atomically precise artificial lattices and graphene nanoribbons, *Adv. Phys.: X* **4**, 1651672 (2019), and references therein.
- [47] Z. Liu, F. Liu, and Y.-S. Wu, Exotic electronic states in the world of flat bands: From theory to material, *Chin. Phys. B* **23**, 077308 (2014).
- [48] D. Leykam, A. Andreev, and S. Flach, Artificial flat band systems: From lattice models to experiments, *Adv. Phys.: X* **3**, 1473052 (2018).